*Int. J. Electrochem. Sci.*, 16 **(2021)** Article ID: 210315, doi: 10.20964/2021.03.11

International Journal of
ELECTROCHEMICAL
SCIENCE
www.electrochemsci.org

# Percolation Micro-Model to Predict the Electrochemical Properties of Composite Anode and Cathode in Protonic Ceramic Fuel Cell

*Zhifei Yuan*[1,2,*], *Hongzhe Zhang*[2], *Jiapei Liu*[2], *Houju Pei*[1]

[1] College of Aerospace Engineering, Nanjing University of Aeronautics and Astronautics, Nanjing 210016, China
[2] School of Energy and Power Engineering, Jiangsu University of Science and Technology, Zhenjiang 212003, China
[*]E-mail: yuan_zhifei@163.com

*Received:* 6 November 2020 / *Accepted:* 23 December 2020 / *Published:* 31 January 2021

As one of the potential alternatives to reduce the operation temperature of solid oxide fuel cell (SOFC) to the intermediate temperature range, protonic ceramic fuel cell ($H^+$-SOFC or PCFC) has received more and more attention. Because there is lower activation energy of protons transport than that of oxygen ions, the vapor is produced within the cathode side instead of anode side. It means that there are different relations among the microstructure parameters, electrode properties and multi-physics working processes within fuel cells, compared with the traditional high temperature $O^{2-}$-SOFC and low temperature proton exchange membrane fuel cell (PEMFC). In this paper, the percolation micro model is adopted to study the effects of the microstructure parameters on the detail effective multi-physics transporting and electrochemical properties of PCFC binary component anode and cathode. It would be helpful to quantitatively understand the influence of microstructure factors on PCFC operation and further apply the understanding to the design and fabrication of composite electrode microstructure as the approach to achieve a high PCFC performance.

**Keywords:** Protonic ceramic fuel cell; Percolation theory; Porous composite electrode microstructure; Multi-physics transporting and electrochemical properties

## 1. INTRODUCTION

Recently, protonic ceramic fuel cell ($H^+$-SOFC or PCFC) has received much attention due to its very different characteristics [1-4], compared with the solid oxide fuel cell (SOFC) operating in high temperature zone (i.e., 600 $^oC$ -800 $^oC$) [5-7] and the proton exchange membrane fuel cell (PEMFC) operating in low temperature zone (i. e., <100 $^oC$). On one hand, PCFCs use the solid ceramic as the dense electrolyte and can directly use hydrocarbon fuels to generate electricity with a conversion

efficiency above 50% [1]. On the other hand, the PCFC that works around intermediate temperature zone (i.e., 200 ºC -500 ºC) can relief the pressures of both the compatibility constraint among the components and operational complexity in high temperature condition [8-10]. Generally, the PCFCs have the following two advantages: a) lower activation energy of proton transport than that of oxygen ions at the intermediate temperature zone [11-13], which means the protonic electric conductivities of these ceramic materials have less temperature dependence compared with most of the oxygen conducting ceramic materials; b) vapor will be generated within the cathode instead of anode zone. Thus, faster fuel transport capability will greatly decrease the concentration polarization loss within the support anode layer, and higher Nernst potential can also be expected [11].

As reported by J. Kim [11], $NdBa_{0.5}Sr_{0.5}Co_{1.5}Fe_{0.5}O_{5+\delta}$ (NBSCF) had the $H^+/O^{2-}/e^-$ triple conducting properties and could effectively extend the electrochemical active sites of PCFC cathode. The $La_{0.4}Sr_{0.6}Co_{0.2}Fe_{0.8}O_{3-\delta}$ - $BaZr_{0.7}Pr_{0.1}Y_{0.2}O_{3-\delta}$ (LSCF-BZCY) and $La_{0.4}Sr_{0.6}Co_{0.2}Fe_{0.8}O_{3-\delta}$ - $Ce_{0.8}Sm_{0.2}O_{1.9}$ (LSCF-SDC) composite cathodes for PCFCs were compared and found that proton electron mixed conducting composite cathode was more suitable than the oxygen ion electron mixed conducting cathodes to serve the PCFCs [14]. S. Choi found that the protonic ceramic electrochemical cells with PBSCF as air electrode, BZCYYb as dense electrolyte and Ni-BZCYYb as fuel electrode could provide high stability and faradaic efficiencies for both the hydrogen production and electricity generation processes [2]. Generally speaking, the porous composite electrodes are considered as the key components to support the energy conversion of PCFC between the chemical and electric energies. Taking the porous composite cathode of PCFC as an example, it is not limited to the following functions; a) providing the continuous paths for the gas, electron, oxygen ions and proton transports, respectively; b) providing the coexistence sites of oxygen, $O^{2-}$ and electron transporting networks to support the oxygen reduction half reaction; c) providing the coexistence sites of $O^{2-}$, proton and vapor transfer paths to support the vapor formation half reaction. In other words, the PCFC performance is a tradeoff of these electric charges and species transporting processes and the electrochemical reactions. The electric charges and species will choose the most convenient path to be transported and converted among each other for achieving the minimal energy drop, which will greatly depend on the compromising among the effective properties of composite electrode. Therefore, studying the effects of the microstructure on the effect physics and electrochemical properties of both the PCFC composite anode and cathode is very important.

In general, the percolation micro model has been considered as the proper approach to present the relations between the microstructure parameters and the effective physics transporting and electrochemical properties of different porous composite mediums. It consists of the coordination number theory and percolation theory. The coordinaiton number theory represents the powder connecting conditions within structure constructed by the random packing reconstruction particles [15]. These coordination numbers would be further related to the effective physics transporting and electrochemical properties of the composite mediums. These relating formulas would be further obtained by the percolation theory. Bouvard [16] and Suzuki [17] proposed the empirical expression to evaluate the coordination numbers of a binary random packing sphere structure from the microstructure parameters. Then, the analytical expressions were further developed by Costamagna [18] to further relate these coordination numbers and the physics and electrochemical properties of

SOFC composite electrodes. Recently, D. Chen [15] further revised the coordination number theory to make it satisfy the contact number conservation principle, and further generalized the percolation micro model to evaluate the effective properties for a LSM particles, coarse YSZ and fine YSZ particles 3-components SOFC composite electrode. Different poly-disperse powder size distributions of composite cathode and anode components were studied, finding that component material with mono-sized particle sizes could increase 32% three phase boundary (TPB) lengths than that with a normal distribution characteristic of particle sizes [19]. Bertei [20] had further investigated the effects of pore former on the SOFC composite electrode by a revised percolation theory. Then, the percolation micro model was further developed to predict the electrochemical properties of a SOFC composite cathode with a mixed electron and oxygen ion conductor (i..e., LSCF-YSZ and LSCF-LSM composite cathodes) [21, 22]. Up to now, the percolation micro models have been widely adopted to predict the effective properties for different composite mediums [23-26]. Additionally, the percolation micro model is widely incorporated into the button cell level model to research on the relation between the electrode microstructures and the fuel cell multi-physics coupling performances [27-32].

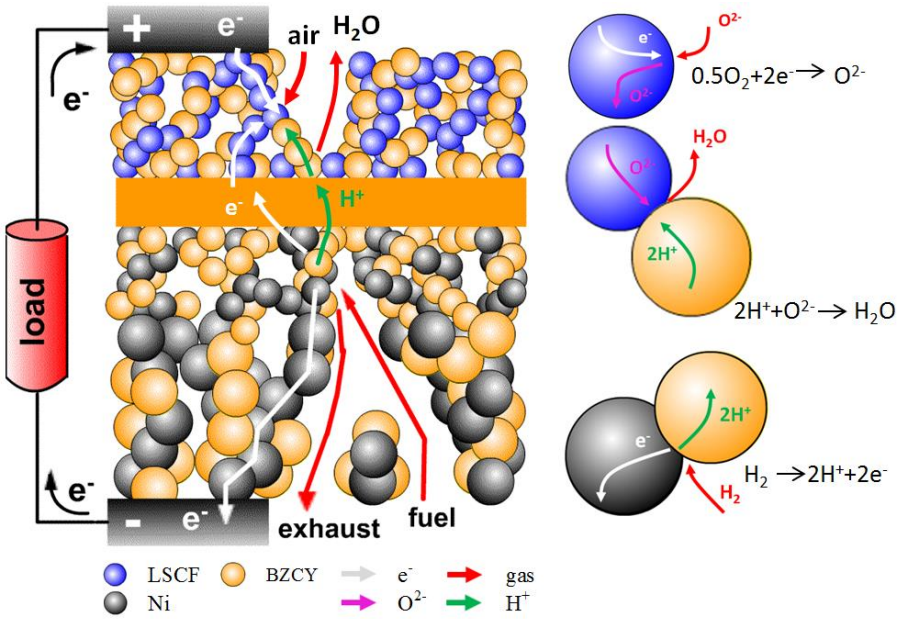


**Figure 1.** The electric charges and species transporting and electrochemical reaction processes within a typical LSCF-BZCY/BZCY/Ni-BZCY protonic ceramic fuel cell.

All of the above research results would greatly increase our understanding on the composite electrodes microstructures, the corresponding transporting and electrochemical properties and fuel cell multi-physics working details. However, to the best of authors' knowledge, there are rare reports about the micro models for the PCFC composite electrodes. Generally, the PCFCs will have different microstructure and properties relationships compared with the traditional $O^{2-}$-SOFC and PEMFC composite electrodes. In this paper, the percolation micro model is adopted to study the effects of the microstructure parameters on the detail effective multi-physics transporting and electrochemical

properties of PCFC binary component anode and cathode. It would improve the understanding of the PCFC composite electrodes on microstructure level.

## 2. PERCOLATION MICRO MODEL FOR THE PCFC COMPOSITE ANODE AND CATHODE

Fig. 1 shows the working processes within a typical Ni-BZCY/BZCY/LSCF-BZCY PCFC to illustrate the functional requirements of the physics transport and electrochemical properties for both the composite anode and cathodes within PCFC. Grey, blue and orange particles present the Ni, LSCF, and BZCY powders, respectively. Similarly, the grey, purple, green and red arrows indicate the electron, oxygen ion, proton and reactant species transfer paths. Although $BaZr_{0.1}Ce_{0.7}Y_{0.2}O_{3-\delta}$ may also present the oxygen ion and electron conducting capabilities, their values are very small, compared with the proton conductivity of BZCY powder, electron conductivity of both LSCF and Ni powders, and the oxygen ion conductivities of LSCF powder, while it is operated around the inter and low temperature regimes [12, 33, 34]. It is reasonable to treat BZCY powders as the pure proton conductors in current study,

For the Ni-BZCY composite anode, the continuous Ni particles network that connect to the anode interconnect will provide the $e^-$ conducting path. Similarly, the continuous BZCY particles network that connect to the dense electrolyte will provide the $H^=$ conducting path. The percolated pores that connects throughout the entire electrode structure will provide the fuel diffusing path. The coexist sites of the electron, proton and pores networks will provide the anodic electrochemical half reaction the triple phase boundary lengths,

$$H_2(\text{pore}) \rightarrow H^+(\text{BZCY}) + 2e^-(\text{Ni}) \qquad (1)$$

where the remarks within parentheses mean the carriers of the corresponding electric charges and reactant species. Apparently, the electrochemical half reaction in Eq. (1) owns the heterogeneous characteristic referring to the $H_2$, $e^-$ and $H^+$.

For the LSCF-BZCY binary components cathode, the continuous LSCF particles network connected to the cathode interconnect will provide the electron conducting path. The continuous LSCF powder network connected to the dense electrolyte directly or by BZCY particles will provide the oxygen ion conducting path. The continuous BZCY particles network connected to the dense electrolyte will provide the $H^=$ conducting path. The percolated pores that connects throughout the entire electrode structure will provide the oxygen and vapor diffusing ways. Different from $O^{2-}$-SOFC, the cathodic electrochemical reactions within PCFC should consist of oxygen reducing half reaction as Eq. (2) and vapor formation half reaction as Eq. (3). Because only the protons can pass through the PCFC dense electrolyte, generally, the oxygen reducing half reaction can be estimated as a function of the oxygen partial pressure $p_{O_2}$ with a reaction order 1/4 [13, 35, 36]. The vapor formation half reaction is a function of vapor partial pressure $p_{H_2O}$ in a reaction order 1/2 [35, 37].

$$0.5O_2(\text{pore}) + 2e^-(\text{LSCF}) \rightarrow O^{2-}(\text{LSCF}) \qquad (2)$$

$$O^{2-}(\text{LSCF}) + 2H^+(\text{BZCY}) \rightarrow H_2O(\text{pore}) \qquad (3)$$

Therefore, balancing the $e^-$, $H^+$, $O^{2-}$ and species transfer properties and the anodic electrochemical active, cathodic oxygen reductive and vapor formatting active sites by adjusting the microstructure parameters is one of the most important steps for achieving the high multi-physics and electrochemical coupling performance processes.

The percolation micro-model is a proper approach to present the relations between the microstructure parameters and the effective physics and electrochemical properties of the PCFC composite electrodes. Firstly, coordination numbers are adopted to characterize the connecting conditions among the different powders within the porous mediums.

Taking the binary components composite electrode as an example, the coordination number between a *k*-powder and all its neighboring powders could be evaluated by,

$$Z_k = \sum_{l=1}^{2} Z_{k,l} \qquad (4)$$

where $Z_{k,l}$ is the average contact number between the *k*-powder and all of its neighboring $l$-powders. It can be evaluated as a function of the microstructure parameters (i.e., electrode component, volume fraction, particle radius and so on) [13, 15],

$$Z_{k,l} = (1 + r_k^2 / r_l^2)\frac{\bar{Z}}{2}\frac{\psi_l / r_l}{\sum_{k=1}^{2}\psi_k / r_k} \qquad (5)$$

where $r_k$ and $\psi_k$ are the radius and solid volume fraction of the *k*-powders, $\bar{Z} = 6$ is the average coordination number of all powders in the random packing structure [38].

The number of *k*-powders per unit volume can be obtained as,

$$n_k^{\mathrm{V}} = \frac{(1-\phi_g)\psi_k}{4\pi r_k^3 / 3}, \ [\mathrm{m}^{-3}] \qquad (6)$$

where $\phi_g$ is the porosity of the porous composite electrode. Then, $n_k^{\mathrm{V}} Z_{k,l}\ (k \neq l)$ and $n_k^{\mathrm{V}} Z_{k,k} / 2$ are the number of *k*-*l* $(k \neq l)$ contacts and *k*-*k* contacts per unit volume.

Secondly, the percolation theory will be used to further connect the coordination numbers to the effective physics transporting and electrochemical properties of the composite electrodes within the PCFC.

For the Ni-BZCY composite anode of PCFC in Fig. 1, the percolated triple phase boundaries among the Ni networks connected to the anode interconnect, BZCY networks connected to the dense electrolyte, and the pores networks connected to the anode channels will provide the active sites for the anodic electrochemical half reaction in Eq. (1),

$$\lambda_{\text{Ni-BZCY-pore}}^{\mathrm{V}} = \gamma_{\mathrm{Ni,BZCY}} n_{\mathrm{Ni}}^{\mathrm{V}} Z_{\mathrm{Ni,BZCY}} P_{\mathrm{Ni}}^{\mathrm{e}} P_{\mathrm{BZCY}}^{\mathrm{H}^+}, \ [\mathrm{m}^{-2}] \qquad (7)$$

where $\gamma_{\mathrm{Ni,BZCY}} = 2\pi r_{\mathrm{c}}$ is the circular length of per Ni-BZCY contact as illustrated in Fig. 2a. $r_{\mathrm{c}} = \min(r_k, r_l)\sin\theta$ can be estimated through the smaller powder radius and contact angle $\theta$.

As illustrated in Equations. (5) and (6), $n_{\mathrm{Ni}}^{\mathrm{V}} Z_{\mathrm{Ni,BZCY}}$ is the overall number of Ni-BZCY contacts per volume of the Ni-BZCY composite anode. $P_{\mathrm{BZCY}}^{\mathrm{H}^+}$ is the probability of the corresponding BZCY particle that belongs to the percolated $H^+$ conducting path throughout the whole anode

structure. Thus, it can be a function of the coordination conditions among the BZCY particles as [13, 39],

$$P_{\mathrm{BZCY}}^{\mathrm{H^+}} = 1 - \left( \frac{4.236 - Z_{\mathrm{BZCY,BZCY}}}{2.472} \right)^{3.7} \qquad (8)$$

As illustrated in Eq. (5), $Z_{k,k}$ is a function of the electrode component, powder radii and volume fraction. There is a threshold value of the volume fraction $\psi_k^{\mathrm{c}}$ for the *k*-particles (i.e., BZCY powders) to construct the percolated network, while the ratios between the *k*- and *l*-powder sizes are chosen;

$$Z_{k,k} = \bar{Z} \frac{\psi_k^{\mathrm{c}} / r_k}{\sum_{l=1}^{2} \psi_l / r_l} = 1.764 \qquad (9)$$

The volume fraction threshold value of the electrode component (i.e., LSCF of BZCY) is an important factor to ensure the high physics transporting and electrochemical properties of a composite electrode. Similarly, the probability of the corresponding Ni-particle belonging to the percolated electronic conducting path throughout the whole anode structure can be estimated by Eq. (8) as $P_{\mathrm{Ni}}^{\mathrm{e^-}} = 1 - \left[ (4.236 - Z_{\mathrm{Ni,Ni}}) / 2.472 \right]^{3.7}$.

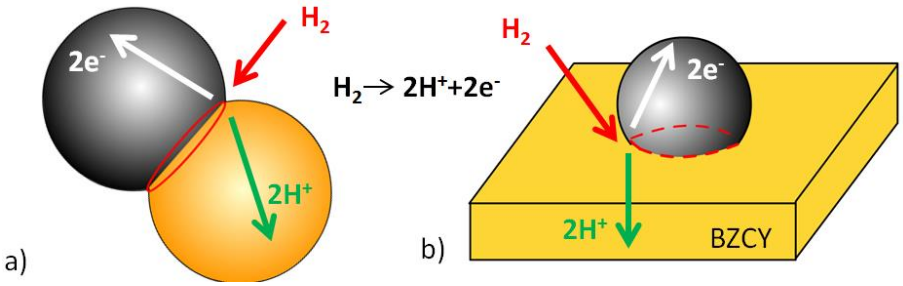


**Figure 2.** Active sites for the anodic electrochemical reaction within the binary component anode and over the dense electrolyte surface.

In addition, as illustrated in Fig. 2b, the percolated Ni-BZCY-pores TPBs over the dense electrolyte surface areas are another important electrochemical active sites to support the anodic electrochemical reaction;

$$\lambda_{\mathrm{Ni\text{-}ele\text{-}pore}}^{\mathrm{S}} = \gamma_{\mathrm{Ni,ele}} n_{\mathrm{Ni}}^{\mathrm{S}} P_{\mathrm{Ni}}^{\mathrm{e^-}}, \ [\mathrm{m^{-1}}] \qquad (10)$$

where the per contact length between a Ni particle and the dense electrolyte surface could be calculated by $\gamma_{\mathrm{Ni,ele}} = 2\pi r_{\mathrm{Ni}} \sin\theta$. The *k*-powder number over per square meters dense electrolyte surface is [19],

$$n_k^{\mathrm{S}} = (1 - \phi_g)\psi_k / (2\pi r_k^2 / 3), \ [\mathrm{m^{-2}}] \qquad (11)$$

For the LSCF-BZCY binary composite cathode in Fig. 1, however, the cathodic electrochemical reactions within PCFC should consist of oxygen reducing half reaction as Eq. (2) and vapor formation half reaction as Eq. (3). LSCF and BZCY are the electron oxygen ion mixed conducting medium and the proton conducting medium, respectively. In other words, $e^-$ and $O^{2-}$ exist

at the LSCF powders; $H^+$ can only be transported by BZCY powder; $O_2$ and vapor are diffused through the porous phase within the LSCF-BZCY binary cathode.

Because LSCF particles have the electronic and oxygen ionic mixed conducting property, the percolated LSCF surfaces that are exposed to the gas phase are potential electrochemical active sites to support the cathodic oxygen reduction in Eq. (2) [13, 22],

$$S^{V}_{es,LSCF} = n^{V}_{LSCF} s_{es} P^{e^-}_{LSCF}, \text{ [m}^{-1}\text{]} \qquad (12)$$

$P^{e}_{LSCF}$ represents the probability of the LSCF particle belonging to both percolated electron and oxygen ion conducting paths within the LSCF-BZCY binary cathode. It can be similarly calculated by Eq. (8). As illustrated in Fig. 3a, $s_{es}$ is the exposed surface area of each LSCF powder. It could be evaluated by subtracting the LSCF spherical surface area with the overlap parts from its neighboring LSCF and BZCY particles [13, 21];

$$s_{es} = 2\pi r^2_{LSCF}[2-(1-\cos\theta_{LSCF})Z_{LSCF,LSCF}-(1-\cos\theta_{LSCF})Z_{LSCF,BZCY}], \text{ [m}^{-1}\text{]} \quad (13)$$

where $\theta_{LSCF}$ is the contact angle between $r_{LSCF}$- and its neighboring $r_2$-powder and $r_{LSCF}\sin\theta_{LSCF} = r_2 \sin\theta_2$ [13, 22].

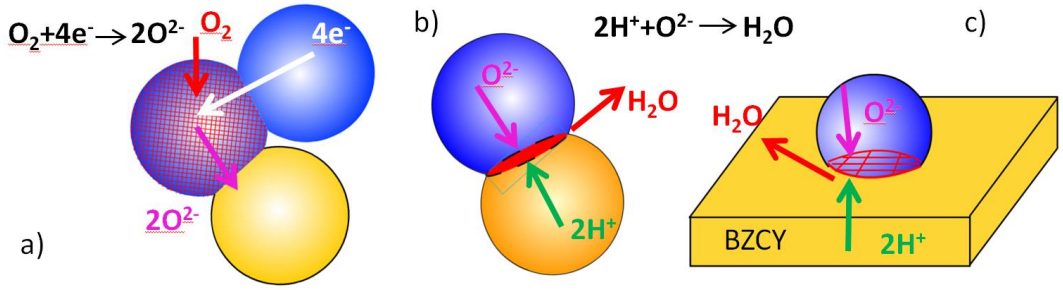


**Figure 3.** Potential active sites for the cathodic reactions; a) percolated LSCF surfaces for the oxygen reducing reaction, b-c) percolated LSCF-BZCY binary phases areas for the vapor producing reactions.

Similarly, the vapor formation half reaction in Eq. (3) implies that the coexist sites of $O^{2-}$, $H^+$ and vapor transfer paths are required. As LSCF and BZCY powders are the oxygen ionic and protonic conducting mediums within the binary composite cathode, respectively, and the percolated LSCF-BZCY double phase contact areas (shown in Fig. 3b) would be the potential active sites for the cathodic vapor formation half reaction,

$$A^{V}_{LSCF\text{-}BZCY} = a_{LSCF,BZCY} n^{V}_{LSCF} Z_{LSCF,\,BZCY} P^{O^{2-}}_{LSCF} P^{H^+}_{BZCY}, \text{ [m}^{-2}\text{]} \qquad (14)$$

As illustrated in Fig. 2b, $a_{LSCF\text{-}BZCY} = \pi r_c^2$ is the cross-sectional areas per BZCY-LSCF contact. $P^{H^+}_{BZCY}$ is the probability of BZCY powders that contributes to the percolated proton conducting network. The percolated $H^+$ conducting path is a key factor to extend the vapor formation half reaction active sites from the dense electrolyte into the composite cathode zone.

Similarly, the percolated LSCF-BZCY double phases contact areas over the cathode/dense electrolyte interface (illustrated in Fig. 3c), could also provide the coexisting sites of oxygen ion,

proton and vapor transfer ways. They are also the potential electrochemical active sites for the vapor formation half reaction as described in Eq. (3),

$$A^{S}_{\text{LSCF-BZCY}} = a_{\text{LSCF,ele}} n^{S}_{\text{LSCF}} P^{O^{2-}}_{\text{LSCF}}, \text{ [m}^{-1}\text{]} \qquad (15)$$

where $a_{\text{LSCF,ele}} = \pi(r_{\text{LSCF}} \sin\theta)^2$ is the contact areas between a LSCF powder and the dense electrolyte. It could be similarly evaluated by Eq. (12).

In addition to the electrochemical properties, the effective multi-physics transporting properties, such as the electrons, oxygen ions, protons electric conductivities and the species diffusivity, are also the important factors to support the energy conversing processes within the PCFC composite electrodes.

Hydraulic radius is an important item to describe the gas diffusing capability within the porous electrode structure [40]. Especially for the PCFC composite cathode, where the vapors are generated within the cathode instead of the anode zone. For the composite electrode with binary components *k*- and *l*-powders, the hydraulic radius of the porous electrode structure could be calculated as [13, 15],

$$r_{\text{g}} = \frac{2}{3} \frac{1}{(1-\phi_{\text{g}}) \sum_{k=1}^{2} \frac{\psi_k}{r_k}}, \text{ [m]} \qquad (16)$$

## 3. RESULT AND DISCUSSION

For a typical Ni-BZCY/BZCY/LSCF-BZCY PCFC, the microstructure parameters on the electrochemical properties of the binary Ni-BZCY anode and LSCF-BZCY cathode will be calculated and studied by the above percolation micro model, respectively.

### *3.1. Threshold volume fraction of the component for percolation*

Threshold volume fraction value is the minimal loading requirement of a component (i.e., Ni, LSCF or BZCY) to structure a network connecting throughout the whole composite electrode structure. Fig. 4 shows the threshold volume fractions of the electronic conducting powder (i.e., Ni or LSCF) and the protonic conducting BZCY powder, while different powder size ratios are adopted.

For $r_{\text{Ni}} / r_{\text{BZCY}} = 0.3, 0.5, 1, 2, 3, 4$, the corresponding Ni powder loadings to construct a percolated electric conducting path are $\psi^{\text{c}}_{\text{Ni}} = 10.1\%$, 17.3%, 29.5%, 45.5%, 54.5% and 62.5%, respectively. The corresponding BZCY powder loadings to construct a percolated protonic conducting path are $\psi^{\text{c}}_{\text{BZCY}} =$ 56.8%, 45.5%, 29.5%, 17.3%, 11.8% and 9.5%, respectively. Thus, it is obvious that while the $r_{\text{Ni}} / r_{\text{BZCY}}$ is chosen, the BZCY powder loading should be limited within the range ($\psi^{\text{c}}_{\text{BZCY}}$ : $(1-\psi^{\text{c}}_{\text{Ni}})$) for ensuring the percolated of both the electronic and protonic conducting paths. This phenomena is observed experimentally, the polarization resistance decrease sharply, while the loading of the electronic conductors reaches the volume fraction value [41].

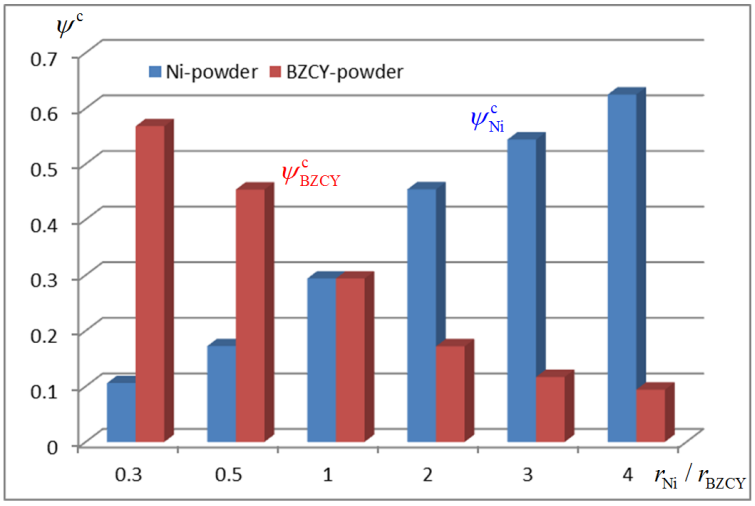


**Figure 4.** The threshold volume fractions of the Ni (or LSCF) powder and BZCY powder, while their particle size ratios are assigned.

*3.2 The electrochemical active sizes of the PCFC composite anode*

Taking the Ni-BZCY composite anode with $\phi_g = 0.4$ as an example, Fig. 5 displays the effects of different Ni volume fraction loading and particle sizes ($r_{Ni}$, $r_{BZCY}$) on the percolated Ni-BZCY-pore TPB lengths per electrode volume $\lambda^V_{TPB,per}$. For $r_{Ni} = r_{BZCY} = 0.5\,\mu m$, the relation between the $\lambda^V_{TPB,per}$ and Ni loading $\psi_{Ni}$ can be obtained from Fig. 5.

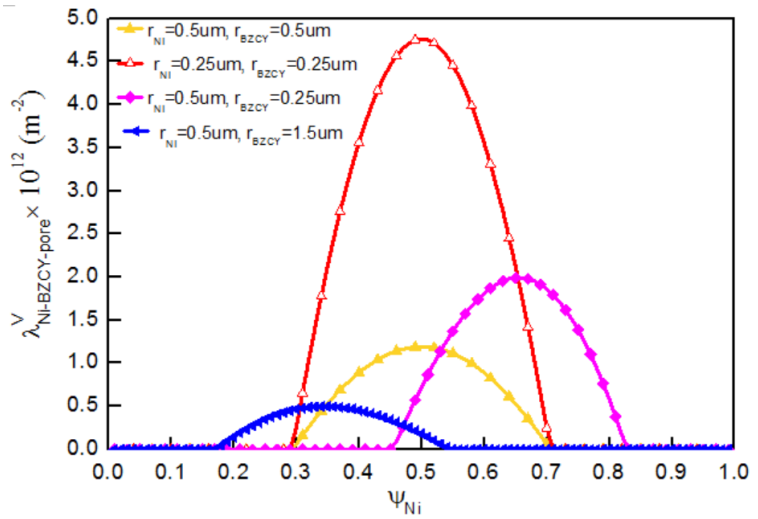


**Figure 5.** Dependence of $\lambda^V_{TPB,per}$ on the Ni volume fraction loading and particle sizes within the Ni-BZCY composite anode.

The maximum value $1.19\times10^{12}$ $m^{-2}$ will appear at $\psi_{Ni} = 50\%$. From Fig. 5, while the particle size decreases a factor 0.5 to $r_{Ni} = r_{BZCY} = 0.25\,\mu m$, the corresponding $\lambda^V_{TPB,per}$ will increase four times.

$\lambda^{V}_{TPB,per}$ is proportional to the particle size $r^2$. Furthermore, while different particle sizes of Ni and BZCY are used ($r_{Ni}/r_{BZCY}=1/3, 2$), the corresponding Ni powder loading values for the maximum $\lambda^{V}_{TPB,per}$ will shift from 50% to 35% and 65%, respectively. This result is similar and consistent with the reported result basing on Ni-YSZ composite anode of solid oxide fuel cells [22].

Similarly, Fig. 6 shows the dependence of the percolated Ni-BZCY-pore TPB lengths over the dense electrolyte surface $\lambda^{S}_{TPB,per}$ on different Ni volume fraction loading and particle size ($r_{Ni}$, $r_{BZCY}$). Obviously, the particle size ratio $r_{Ni}/r_{BZCY}$ is the key factor to determine the start value of the effective Ni-BZCY-pore TPB lengths over the electrolyte surface, because it will determine the threshold volume of the Ni powder loading. Additionally, the practical Ni particle size is an important factor to affect the value of $\lambda^{S}_{TPB,per}$. $\lambda^{S}_{TPB,per}$ is proportional to the $r_{Ni}$. As shown in Fig. 6, while $r_{Ni}=r_{BZCY}=0.5\,\mu m$ is decreased to $r_{Ni}=r_{BZCY}=0.25\,\mu m$, $\lambda^{S}_{TPB,per}$ will be increased from $9.22\times10^5$ $m^{-1}$ to $18.44\times10^5$ $m^{-1}$.

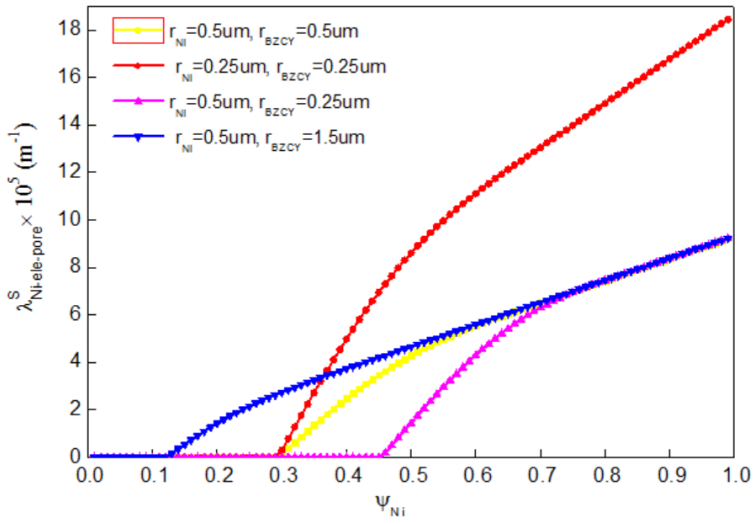


**Figure 6.** Dependence of $\lambda^{S}_{TPB,per}$ on different Ni volume fraction loading and particle sizes within the Ni-BZCY composite anode.

### *3.3 The electrochemical active sizes of the PCFC composite cathode*

For the PCFC composite cathode (i.e., LSCF-BZCY), however, the electrochemical reactions will be divided into two steps: a) oxygen will be diffused to the LSCF surface and reacted with the electrons to produced oxygen ions; b) oxygen ions should be conducted to the LSCF-BZCY binary phases boundaries and reacted with the protons.

Fig. 7 shows the dependence of the percolated exposed LSCF surfaces $S^{V}_{es,LSCF}$ on different LSCF volume fraction loading and particle sizes within the LSCF-BZCY composite cathode. Obviously, $S^{V}_{es,LSCF}$ should keep increasing with the increase LSCF powder loading. For the $r_{Ni}=r_{BZCY}=0.5\,\mu m$ and $\phi_g=0.4$ case, the maximum $S^{V}_{es,LSCF}=2.176\times10^6$ $m^{-1}$ would be achieved at the point $\psi_{LSCF}=100\%$. Furthermore, decreasing the LSCF particle size by one time should increase the

$S^{V}_{es,LSCF}$ value by one time. This conclusion is also consistent with the calculated result reported by D. Chen [13].

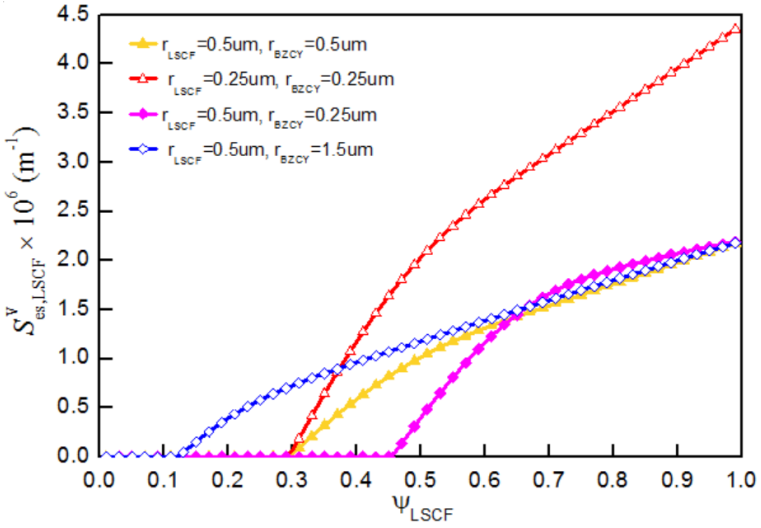


**Figure 7.** Dependence of $S^{V}_{es,LSCF}$ on different LSCF volume fraction loading and particle sizes within the LSCF-BZCY binary composite cathode.

Fig. 8 further shows the calculated percolated LSCF-BZCY double phases contact areas per electrode volume $A^{V}_{LSCF\text{-}BZCY}$ with different LSCF powder loading and particle sizes. Obviously, the effective $A^{V}_{LSCF\text{-}BZCY}$ will be restricted within the LSCF powder loading range ($\psi^{c}_{LSCF}$ : $(1-\psi^{c}_{BZCY})$). As illustrated in Fig. 4, $\psi^{c}_{LSCF}$ and $\psi^{c}_{BZCY}$ are the minimal volume fraction loadings for the LSCF and BZCY powders to construct the percolated connecting networks, respectively.

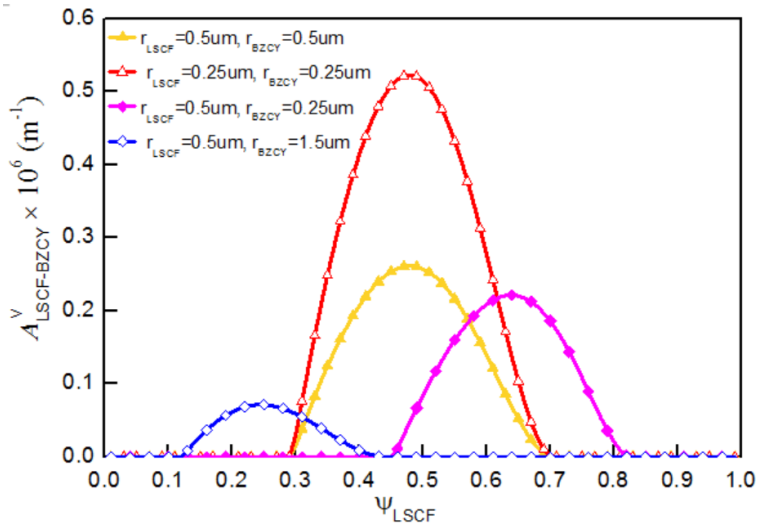


**Figure 8.** further shows the calculated percolated LSCF-BZCY double phases contact areas per electrode volume with different LSCF powder loading and particle sizes.

For the $r_{Ni}=r_{BZCY}=0.5\,\mu m$ case, the maximal $A^{V}_{LSCF\text{-}BZCY}=0.257\times10^{6}$ $m^{-1}$ would be achieved at the point $\psi_{LSCF}=50\%$; and it will be increased to $0.515\times10^{6}$ $m^{-1}$, while the smaller particle size $r_{Ni}=r_{BZCY}=0.25\,\mu m$ is adopted. Generally, $A^{V}_{LSCF\text{-}BZCY}$ is inversely proportional to particle size by one time. While ($r_{Ni}=0.5$, $r_{BZCY}=0.25\,\mu m$) and ($r_{Ni}=0.5$, $r_{BZCY}=1.5\,\mu m$) are used, the maximal $A^{V}_{LSCF\text{-}BZCY}=0.222\times10^{6}$ and $0.072\times10^{6}$ $m^{-1}$ will appease around the points $\psi_{LSCF}=64\%$ and 24%, respectively.

Similarly, Fig. 9 further shows the calculated percolated LSCF-electrolyte contact areas per unit dense electrolyte surface $A^{S}_{LSCF\text{-}ele}$ as a function of the LSCF powder loading and powder sizes. Obviously, for the ($r_{LSCF}=r_{BZCY}=0.5\,\mu m$) and ($r_{LSCF}=r_{BZCY}=0.25\,\mu m$), there are similar $A^{S}_{LSCF\text{-}ele}$~$\psi_{LSCF}$ relation curve. $A^{S}_{LSCF\text{-}ele}$ will be decreased with decreasing LSCF powder loading. For the ($r_{LSCF}$=0.5, $r_{BZCY}$=1.5 μm, $r_{LSCF}/r_{BZCY}$=1/3) case, the effective $A^{S}_{LSCF\text{-}ele}$ will be extended to the range from $\psi_{LSCF}$=13~100%. For the ($r_{LSCF}$=0.5, $r_{BZCY}$=0.25 μm, $r_{LSCF}/r_{BZCY}$=2) case, however, the effective $A^{S}_{LSCF\text{-}ele}$ will be reduced to the range from $\psi_{LSCF}$=46~100%.

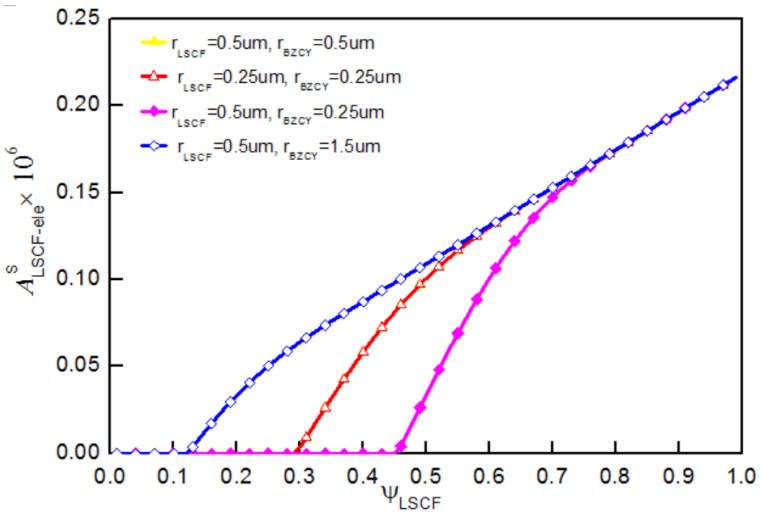


**Figure 9.** The calculated percolated LSCF-electrolyte contact areas per unit dense electrolyte surface as a function of the LSCF powder loading and powder sizes.

Fig. 10 further shows the calculated hydraulic radius $r_g$ as a function of *ed*-powder (i.e., Ni or LSCF in current cases) at ($r_{LSCF}=r_{BZCY}$=0.5 μm), ($r_{LSCF}=r_{BZCY}$=0.25 μm), ($r_{LSCF}$=0.5, $r_{BZCY}$=0.25 μm) and ($r_{LSCF}$=0.5, $r_{BZCY}$=1.5 μm) cases. Obviously, for the *ed*- and BZCY powders with the same particle sizes, the hydraulic radials of the porous electrode structure $r_g$ are 0.556 and 0.278 μm for the ($r_{LSCF}=r_{BZCY}$=0.5 μm) and ($r_{LSCF}=r_{BZCY}$=0.25 μm) cases, respectively. For the ($r_{LSCF}$=0.5 μm, $r_{BZCY}$=0.25 μm) case, $r_g$ will increase with the increasing *ed*- powder loading from 0.28 to 0.55 μm. For the ($r_{LSCF}$=0.5 μm, $r_{BZCY}$=1.5 μm), however, $r_g$ will decrease with the increasing *ed*- powder loading from 1.63 to 0.56 μm.

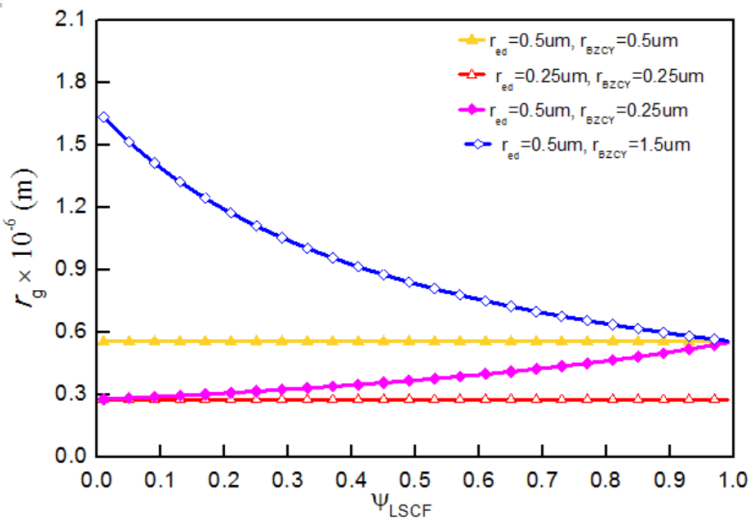


**Figure 10.** The calculated hydraulic radius as a function of *ed*-powder at different particle sizes cases.

## 4. CONCLUSIONS

In this paper, the percolation micro model has been adopted and generalized to study the influences of the microstructure parameters on the effective electrochemical properties of the Ni-BZCY and LSCF-BZCY composite electrodes within a full PCFC. Parts of the research results can be concluded as follows.

For the Ni-BZCY composite anode of PCFC, the percolated Ni-BZCY-pore TPBs per electrode volume $\lambda^{V}_{TPB,per}$ was found to be inversely proportional to the particle size $r^2$ by two times. The percolated Ni-BZCY-pore TPBs over the anode/dense electrolyte interface $\lambda^{S}_{TPB,per}$ was found to be inversely proportional to the powder size $r$ by one time. The Ni powder loading corresponding to the maximal $\lambda^{V}_{TPB,per}$ would be changed according to the different $r_{Ni}/r_{BZCY}$ ratios.

For the LSCF-BZCY composite cathode of PCFC, the percolated exposed LSCF surfaces per electrode volume $S^{V}_{es,LSCF}$ for the oxygen reducing reaction was found to be inversely proportional to the powder size $r$. The BZCY powder size would also affect the effective LSCF powder loading zone for the effective $S^{V}_{es,LSCF}$ value. The percolated LSCF-BZCY double phases boundaries per electrode volume $A^{V}_{LSCF\text{-}BZCY}$ for the vapor producing reaction was also found to be proportional to the powder size by one time. The LSCF powder loading corresponding to the maximal $A^{V}_{LSCF\text{-}BZCY}$ would be changed according to the different $r_{LSCF}/r_{BZCY}$ ratios. The percolated LSCF-electrolyte contact areas per unit dense electrolyte surface $A^{S}_{LSCF\text{-}ele}$ would not be affected by the particle sizes, and could be adjusted by changing the LSCF powder loading and $r_{Ni}/r_{BZCY}$ ratios.

The above developed percolation micro model would be helpful for the researchers to understand and guide the design and fabrication of microstructure to achieve high PCFC performance.

ACKNOWLEDGEMENTS
This research was funded by Key Laboratory of Aircraft environment control and life support, MIIT, Nanjing University of Aeronautics & Astronautics, and the financial support of the National Natural Science Foundation of China (51776092), Ministry of Science and Technology of China (CU03-10).

## References

1. C. Duan, R.J. Kee, H. Zhu, C. Karakaya, Y. Chen, S. Ricote, A. Jarry, E.J. Crumlin, D. Hook, R. Braun, N.P. Sullivan, R. O'Hayre, *Nature*, 557 (2018) 217.
2. S. Choi, T.C. Davenport, S.M. Haile, *Energy Environ. Sci.*, 12 (2019) 206.
3. T. Li, T.M.M. Heenan, M.F. Rabuni, B. Wang, N.M. Farandos, G.H. Kelsall, D. Matras, C. Tan, X. Lu, S.D.M. Jacques, D.J.L. Brett, P.R. Shearing, M. Di Michiel, A.M. Beale, A. Vamvakeros, K. Li, *Nat. Commun.*, 10 (2019) 1497.
4. C. Duan, R. Kee, H. Zhu, N. Sullivan, L. Zhu, L. Bian, D. Jennings, R. O'Hayre, *Nat. Energy*, 4 (2019) 230.
5. D. Chen, Y. Xu, M.O. Tade, Z. Shao, *ACS Energy Lett.*, 2 (2017) 319.
6. H. Chen, F. Wang, W. Wang, D. Chen, S.-D. Li, Z. Shao, *Appl. Energy*, 179 (2016) 765.
7. D. Chen, Y. Xu, B. Hu, C. Yan, L. Lu, *Energy Convers. Manage.*, 171 (2018) 807.
8. E.D. Wachsman, K.T. Lee, *Science*, 334 (2011) 935.
9. D. Han, H. Wu, J. Li, S. Wang, Z. Zhan, *J. Power Sources*, 246 (2014) 409.
10. B. Hua, W. Zhang, M. Li, X. Wang, B. Chi, J. Pu, J. Li, *J. Power Sources*, 247 (2014) 170.
11. J. Kim, S. Sengodan, G. Kwon, D. Ding, J. Shin, M. Liu, G. Kim, *Chemsuschem*, 7 (2014) 2811.
12. L. Yang, Z. Liu, S. Wang, Y. Choi, C. Zuo, M. Liu, *J. Power Sources*, 195 (2010) 471.
13. D. Chen, Q. Zhang, L. Lu, V. Periasamy, M.O. Tade, Z. Shao, *J. Power Sources*, 303 (2016) 305.
14. Y. Ling, F. Wang, L. Zhao, X. Liu, B. Lin, *Electrochim. Acta*, 146 (2014) 1.
15. D. Chen, Z. Lin, H. Zhu, R.J. Kee, *J. Power Sources*, 191 (2009) 240.
16. D. Bouvard, F.F. Lange, *Acta Mater.*, 39 (1991) 3083.
17. M. Suzuki, T. Oshima, *Powder Technol.*, 35 (1983) 159.
18. P. Costamagna, P. Costa, V. Antonucci, *Electrochim. Acta*, 43 (1998) 375.
19. D. Chen, L. Lu, J. Li, Z. Yu, W. Kong, H. Zhu, *J. Power Sources*, 196 (2011) 3178.
20. A. Bertei, C. Nicolella, *J. Power Sources*, 196 (2011) 9429.
21. D. Chen, H. He, D. Zhang, H. Wang, M. Ni, *Energies*, 6 (2013) 1632.
22. D. Chen, H. Wang, S. Zhang, M.O. Tade, Z. Shao, H. Chen, *Aiche J.*, 61 (2015) 3786.
23. H. Geistlinger, S. Mohammadian, *Adv.Water Resour.*, 79 (2015) 35.
24. B. Ding, C. Li, M. Zhang, F. Ji, X. Dong, *Chem. Eng. Sci.*, 127 (2015) 40.
25. O. Cekmer, S. Um, M.M. Mench, *Int. J. Heat Mass Transfer*, 86 (2015) 101.
26. A. Bertei, B. Nucci, C. Nicolella, *Chem. Eng. Sci.*, 101 (2013) 175.
27. M.M. Hussain, X. Li, I. Dincer, *Int. J. Hydrogen Energy*, 34 (2009) 3134.
28. D.H. Jeon, J.H. Nam, C.J. Kim, *J. Electrochem. Soc.*, 153 (2006) A406.
29. H.Y. Zhu, R.J. Kee, *J. Electrochem. Soc.*, 155 (2008) B715.
30. B. Völker, R.M. McMeeking, *J. Power Sources*, 215 (2012) 199.
31. D. Chen, B. Hu, K. Ding, C. Yan, L. Lu, *Energies*, 11 (2018) 1875.
32. Kai Ding, Mingfeng Zhu, Zhen Han, Vladimir Kochetov, Liu Lu, D. Chen, *Ionics*, (2020).
33. L. Yang, S. Wang, K. Blinn, M. Liu, Z. Liu, Z. Cheng, M. Liu, *Science*, 326 (2009) 126.
34. C. Zuo, S. Zha, M. Liu, M. Hatano, M. Uchiyama, *Adv. Mater.*, 18 (2006) 3318.
35. R. Peng, T. Wu, W. Liu, X. Liu, G. Meng, *J. Mater. Chem.*, 20 (2010) 6218.
36. H. Uchida, S. Tanaka, H. Iwahara, *J. Appl. Electrochem.*, 15 (1985) 93.
37. H. Yamaura, T. Ikuta, H. Yahiro, G. Okada, *Solid State Ionics*, 176 (2005) 269.
38. S.H. Chan, X.J. Chen, K.A. Khor, *J. Electrochem. Soc.*, 151 (2004) A164.

39. A. Bertei, C. Nicolella, *Powder Technol.*, 213 (2011) 100.
40. W. Kong, H. Zhu, Z. Fei, Z. Lin, *J. Power Sources*, 206 (2012) 171.
41. T. Kawada, N. Sakai, H. Yokokawa, M. Dokiya, M. Mori, T. Iwata, *Solid State Ionics*, Part 1 (1990) 402.